

Imprints of primordial non-Gaussianities in X-ray and SZ signals from galaxy clusters

M. Roncarelli¹, L. Moscardini^{2,3}, E. Branchini⁴, K. Dolag⁵, M. Grossi⁵, F. Iannuzzi⁵ and S. Matarrese^{6,7}

¹ Centre d'Etude Spatiale des Rayonnements, CNRS/Université de Toulouse, 9 avenue du Colonel Roche, BP44346, 31028 Toulouse Cedex 04, France (mauro.roncarelli@cesr.fr)

² Dipartimento di Astronomia, Università di Bologna, via Ranzani 1, I-40127 Bologna, Italy (lauro.moscardini@unibo.it)

³ INFN – Sezione di Bologna, viale Berti Pichat 6/2, I-40127 Bologna, Italy

⁴ Dipartimento di Fisica, Università di Roma TRE, via della Vasca Navale 84, I-00146, Roma, Italy (branchin@fis.uniroma3.it)

⁵ Max-Planck-Institut für Astrophysik, Karl-Schwarzschild Strasse 1, D-85741 Garching bei München, Germany (kdolag,margot,iannuzzi@mpa-garching.mpg.de)

⁶ Dipartimento di Fisica "G. Galilei", Università di Padova, via Marzolo 8, I-35131, Padova, Italy (sabino.matarrese@pd.infn.it)

⁷ INFN – Sezione di Padova, via Marzolo 8, I-35131, Padova, Italy

Accepted ???. Received ???; in original September 2009

ABSTRACT

Several inflationary models predict the possibility that the primordial perturbations of the density field may contain a degree of non-Gaussianity which would influence the subsequent evolution of cosmic structures at large scales. In order to study their impact, we use a set of three cosmological DM-only simulations starting from initial conditions with different levels of non-Gaussianity: $f_{\text{NL}} = 0, \pm 100$. More specifically, we focus on the distribution of galaxy clusters at different redshifts and, using suitable scaling relations, we determine their X-ray and SZ signals. Our analysis allows us to estimate the differences in the $\log N$ - $\log S$ and $\log N$ - $\log Y$ due to the different initial conditions and to predict the cluster counts at different redshifts expected for future surveys (*eROSITA* and *SPT*). We also use a second set of simulations assuming a different cosmological scenario to estimate how the dependence on f_{NL} is degenerate with respect to other parameters. Our results indicate that the effects introduced by a realistic amount of primordial non-Gaussianity are small when compared to the ones connected with current uncertainties in cosmological parameters, particularly with σ_8 . However, if future surveys will be associated with optical follow-up campaigns to determine the cluster redshift, an analysis of the samples at $z > 1$ can provide significant constraints on f_{NL} . In particular we predict that the *SPT* cluster survey will be able to detect ~ 1000 clusters at $z > 1$ for the Gaussian case, with a difference of 15–20 per cent associated to $f_{\text{NL}} = \pm 100$.

Key words: cosmology: theory – (cosmology:) large-scale structure of Universe – galaxies: clusters: general – X-rays: galaxies: clusters – methods: N -body simulations – methods: statistical.

1 INTRODUCTION

The universally accepted scenario for the formation of cosmic structures in the universe is based on the mechanism of gravitational instability, which assumes that the density fluctuations generated at some early epoch grow by accreting mass from the surrounding regions through gravitational processes. The origin of these cosmological seeds is generally related to the final phases of the inflationary expansion for which a large variety of theoretical models exist in the literature (see, e.g., Kinney 2008; Langlois 2008; Baumann & Peiris 2008; Baumann 2009, for recent reviews). These models originate perturbations having different statistical

properties, usually investigated in terms of probability distribution function (PDF) and correlation functions/power polyspectra. In particular, the most standard slow-rolling models, where a single field is responsible for the inflationary accelerated expansion, produce fluctuations having almost uncorrelated phases. For this reason in cosmological studies it is usual to assume that the primordial perturbations are Gaussianly distributed, which leads to the further simplification that their complete description is possible using the power spectrum only. However, even the simplest inflationary models allow for small departures from Gaussianity, which can become more significant in non-standard models, like the scenarios based

on the curvaton, the inhomogeneous reheating and the Dirac-Born-Infeld inflation (see Bartolo et al. 2004, and references therein). As a consequence, the observational determination of the amount of non-Gaussianity present in the primordial fluctuations is now considered not only a general probe for the inflationary concept, but also a powerful discriminatory test between its various theoretical models.

Given the infinite variety of possible non-Gaussian models, it is necessary to introduce a simple way to quantify the level of primordial non-Gaussianity. In the recent years it has become standard practice to adopt the dimensionless non-linearity parameter f_{NL} (see Salopek & Bond 1990; Gangui et al. 1994; Verde et al. 2000; Komatsu & Spergel 2001), measuring the importance of the quadratic term in a sort of Taylor expansion of the Bardeen's gauge-invariant potential Φ , namely

$$\Phi = \Phi_{\text{L}} + f_{\text{NL}}(\Phi_{\text{L}}^2 - \langle \Phi_{\text{L}}^2 \rangle) \quad (1)$$

here Φ_{L} represents a Gaussian random field. In particular, in this paper we follow the so-called large-scale structure (LSS) convention, where Φ , that on scales smaller than the Hubble radius corresponds to the usual Newtonian peculiar potential (but with changed sign), is linearly extrapolated to the present epoch.

For many years, the study of the statistical properties of the cosmic microwave background (CMB) has been considered the most efficient way to measure f_{NL} . In fact its temperature fluctuations are directly related to the density perturbations in a regime in which the non-linearities originated by the subsequent process of gravitational instability are not modifying their primordial characteristics, including the PDF. Different statistical estimators have been applied to the most recent data, keeping improving constraints on f_{NL} . So far the more stringent results come from the analyses of the 5-years *WMAP* dataset: assuming a local shape for non-Gaussianity (as we will do in this paper), Komatsu et al. (2009) found that f_{NL} varies between -12 and 145, while Smith et al. (2009) found $-5 < f_{\text{NL}} < 104^1$ (see also the positive detection of non-Gaussian features reported by Yadav & Wandelt 2008).

More recently it became clear that the LSS represent an alternative tool, potentially as valid as the CMB to constrain f_{NL} . In fact, deviations from an initial Gaussianity induce a different timing for the whole process of structure formation, providing an interesting framework to look for specific non-Gaussian imprints. In general, as already evident from the results of the first generation of non-Gaussian N -body simulations in the early '90s (Messina et al. 1990; Moscardini et al. 1991; Weinberg & Cole 1992), if the primordial density field is positively (negatively) skewed, the formation is favored (disfavoured) and structures of a given mass form at earlier (later) epochs. However, there is an important difficulty in using LSS for constraining f_{NL} : the late non-linear evolution introduces additional non-Gaussian features that need to be disentangled from the primordial ones. For this reason it has been necessary to have resort to suitable high-resolution N -body simulations to follow the growth of the LSS also in the full non-linear regime, and to calibrate the expected signatures as a function of the primordial non-Gaussianity. This has been extensively done in the recent years by different groups (see, e.g., Kang et al. 2007; Grossi et al. 2007; Dalal et al. 2008; Viel et al. 2009; Desjacques et al. 2009; Pillepich et al. 2008; Grossi et al. 2009). The results allowed to assess the power of LSS as inde-

pendent probe for f_{NL} , in particular they showed that the most evident non-Gaussian signatures are present in the mass function and clustering (bias and bispectrum) of dark matter mass haloes (see also the analytical predictions made by Matarrese et al. 2000; LoVerde et al. 2008; Afshordi & Tolley 2008; Carbone et al. 2008; McDonald 2008; Maggiore & Riotto 2009; Lam & Sheth 2009; Valageas 2009; Verde & Matarrese 2009). The first attempts of an application to real data gave very encouraging constraints: Slosar et al. (2008), combining the bias measurements for two samples of luminous red galaxies and quasars, found $f_{\text{NL}} = 37_{-57}^{+42}$, while Afshordi & Tolley (2008), studying the integrated Sachs-Wolfe effect (ISW) in the NVSS survey, derived $f_{\text{NL}} = 272 \pm 127$; error bars are at 2- σ level. Notice that in both cases we report the values as revised by Grossi et al. (2009) to include a correction mimicking the ellipsoidal collapse.

Being at the top of the hierarchy of structure formation, galaxy clusters are in principle ideal probes for constraining f_{NL} . Indeed, the statistics of rare events, either galaxy clusters or deep voids (Viel et al. 2009) are very sensitive to primordial non-Gaussianity. However, until now the use of clusters as non-Gaussian probes has been hampered by two practical problems: first, the observational estimate of their mass is affected by large uncertainties, whatever are the method and the observational band adopted; second, it is difficult to build up samples that span a large range of redshift and are also statistically complete. The first problem can be in some way overcome by using the scaling relations (expected from theoretical arguments and confirmed by observations) existing between mass and different observables (see below). The second problem will be solved in the next years, thanks to the efforts of a set of (in progress or planned) surveys, which promise to provide large samples of galaxy clusters covering a volume comparable to the horizon size: see, e.g., DES, PanSTARRS, BOSS, LSST, ADEPT, EUCLID.

In this paper we will focus on estimating the signals produced by galaxy clusters in the X-ray band and through the Sunyaev-Zel'dovich (SZ, Sunyaev & Zel'dovich 1972, 1980) effect in different non-Gaussian scenarios. We will take advantage of the fact that, in both cases, the corresponding observables, i.e. the X-ray luminosity and the Compton y -parameter, are related to the mass by well calibrated scaling relations. This will allow us to introduce selection criteria mimicking the characteristics of specific surveys. In particular we will consider the properties of the wide surveys planned with *eROSITA* (Predehl et al. 2007) and *SPT* (Carlstrom et al. 2009), as examples of future X-ray and SZ projects, respectively. The main goal of this work is to figure out what are the observational evidences of the presence of some level of primordial non-Gaussianity, discussing the possibility of constraining f_{NL} with these future datasets. Notice that the same samples have been considered for a similar work in Sefusatti et al. (2006); Oguri (2009); Fedeli et al. (2009). In this paper we address this problem using numerical rather than analytical tools. The advantage is twofold. First of all, N -body simulations permit to fully account for non-linear evolution which, instead, is usually accounted for by analytical models in an approximate way only. Second, numerical experiments allow us to extract realistic mock cluster catalogs that can be easily used for modeling the observational selection, which is more difficult to account for in a Fisher matrix-like approach.

The plan of this work is as follows. In Section 2 we present the numerical simulations of non-Gaussian models on which the following analysis is based; we also describe the method applied to construct the light cones. Section 3 introduces our model for the

¹ We multiplied by a factor of 1.3 the original results to convert them to the f_{NL} LSS-convention adopted here.

X-ray emission from galaxy clusters and reports the corresponding results in terms of number counts, paying attention to the expected results for the *eROSITA* wide survey. Section 4 is devoted to the model for the SZ signal and to the corresponding results, given in terms of source counts and statistical properties of the maps; the specific case of the *SPT* wide survey is treated. Section 5 discusses the possibility of using the differential redshift distribution to constrain the primordial f_{NL} . Finally, in Section 6 we draw our conclusions.

2 MODELS AND METHOD

2.1 The simulation sets

In order to study the possibility of detecting the signatures of primordial non-Gaussianity in the LSS of the Universe we must take into account the complete process of structure formation. For this we make use of the outputs of two different sets of DM-only simulations, focusing on the distribution of the DM haloes associated to the galaxy clusters, as identified in the different snapshots.

The first simulation set (presented in Grossi et al. 2009) consists of three DM-only simulations performed with different levels of primordial non-Gaussianity, that, expressed in terms of the dimensionless non-linearity parameter f_{NL} , are $f_{\text{NL}}=0, \pm 100$; the case $f_{\text{NL}}=0$ corresponds to the standard Gaussian case. The initial conditions were set by assuming a flat Λ CDM model dominated by a cosmological constant with parameters chosen to be consistent with the *WMAP* three-year results (Spergel et al. 2007, *WMAP-3* hereafter): namely, the density contributions of cosmological constant and matter correspond to $\Omega_{\Lambda}=0.76$ and $\Omega_{\text{m}}=0.24$, respectively, while the normalization of the power spectrum of density fluctuations is fixed as $\sigma_8=0.8$, being σ_8 the r.m.s. matter fluctuation into a sphere of radius $8h^{-1}$ Mpc. The three simulations started from the same random generation of initial conditions with the only difference consisting in the different value of f_{NL} . All the runs, carried out with the *N*-body code *GADGET-2* (Springel et al. 2001; Springel 2005), followed the evolution of 960^3 DM particles inside a cubic volume of $1200h^{-1}$ Mpc per side, with each particle having a mass of $m = 1.4 \times 10^{11} h^{-1} M_{\odot}$; here h represents the Hubble parameter defined as $h \equiv H_0 / (100 \text{ km s}^{-1} \text{ Mpc}^{-1}) = 0.7$. The gravitational force has been computed using a Plummer equivalent softening length $\epsilon = 25h^{-1}$ kpc.

These simulations produced 14 outputs in the redshift range $0 \leq z \leq 4$. For each snapshot we produced a catalogue of DM haloes identified using a *friends-of-friends* (FOF) algorithm, adopting a linking length of 0.2 times the mean interparticle distance: with this choice the size of the haloes roughly corresponds to their virial mass, M_{vir} . Since in this work we are interested in the X-ray and SZ signals produced by galaxy groups and clusters, we only considered DM haloes having $M_{\text{vir}} > 10^{13} h^{-1} M_{\odot}$. For each halo we kept the information on the mass and the position of its center inside the cosmological volume.

The second set of simulations is the one described in Grossi et al. (2007). It consists on 7 runs covering a wider range of non-Gaussianity: $f_{\text{NL}}=0, \pm 100, \pm 500, \pm 1000$. The main differences with respect to the first set are that the box size is only $500h^{-1}$ Mpc with 800^3 particles and that the cosmological model adopted is close to a *WMAP* first-year (Spergel et al. 2003, *WMAP-1* hereafter) cosmology, with the following cosmological parameters: $\Omega_{\Lambda}=0.7$, $\Omega_{\text{m}}=0.3$, $\sigma_8=0.9$. For this set we have 21 outputs in the range $0 \leq z \leq 4$ and a halo catalogue for each snapshot obtained in the same way as described before and with the same mass

limit. Notice that in this paper this last set of simulations will be mainly used to test the impact of different cosmological parameters compared to non-Gaussianity: for this reason we will discuss only the results of the most extreme and the Gaussian model ($f_{\text{NL}}=0, \pm 1000$). This simulation set will also be used in order to check the effect of the finite box size on our results.

2.2 Constructing the light-cones

As said in Section 1, in order to study the impact of primordial non-Gaussianity on the LSS we adopt an observationally-oriented approach. To this purpose we use the halo catalogues described in Section 2.1 to produce mock light-cones by stacking several simulation volumes. In particular we want to cover the redshift range $0 \leq z \leq 4$, which corresponds to a comoving distance of $5249 h^{-1}$ Mpc ($5019 h^{-1}$ Mpc with the cosmology adopted for the second set). This length requires to stack 5 (11 for the second set) times the simulation box. However, in order to obtain a better redshift sampling, we divide the simulation volume into slices along the line of sight. The number of slices varies from cube to cube and their comoving distance intervals are created in order to allow us to use all of the 14 (21 for the second set) snapshots. More precisely, for any given distance from the observer we compute the corresponding time elapsed from the big bang and we choose the snapshot that better approximates this value.

In order to avoid the repetition of the same structures along the line of sight, for every stacked simulation volume we perform a randomization of the halo spatial coordinates: for every cube we randomly choose the axis to put along the line of sight, we assign a 50 per cent probability to reflect each axis and, since our simulations assume periodic boundary conditions, we proceed to a random recentering of the coordinates. In order to preserve the whole information on the structures inside the simulations' volume, the slices belonging to the same cube undergo the same randomization process. With this method, which is similar to the one adopted by Roncarelli et al. (2006a), we obtain 18 different slices belonging to 5 independently randomized cubes (31 and 11 for the second simulation set, respectively). This process is repeated with the same initial random seed for all the simulations of the set. Each light-cone produced in this way spans an angle of 13.1 deg (5.71 deg for the second set) per side, determined by the length of the box at the maximum redshift, $z = 4$.

By varying the initial random seeds we can obtain different light-cone realizations that we can use to assess the statistical robustness of our results. For each non-Gaussian model, we created 20 (100) different light-cone realizations, thus covering a total area of 3432 deg^2 (3260 deg^2). However, it is important to note that this area cannot be considered as completely independent, being produced starting from the same finite volume of the simulation: as a reference, at $z \simeq 4$ the same simulation volume is completely stacked in all realisations, while at $z \simeq 0.5$ we are able to produce about 15 independent volumes crossing the light-cones.

Using the whole set of light-cone realizations we compute the mass functions, expressed in terms of number of objects per solid angle, for 4 redshift bins. We show in Fig. 1 the results for the three models of the first set ($f_{\text{NL}}=0, \pm 100$) and for the $f_{\text{NL}}=0, \pm 1000$ models of the second set.

Looking at the $0 \leq z \leq 0.5$ bin, the three mass functions of the first set are basically indistinguishable. The non-Gaussian deviations become more evident in the tail at higher masses and at higher redshifts: in the second bin ($0.5 \leq z \leq 1$) the $f_{\text{NL}} = \pm 1000$ models introduce a ± 5 per cent difference in the high mass ($M_{\text{vir}} \gtrsim$

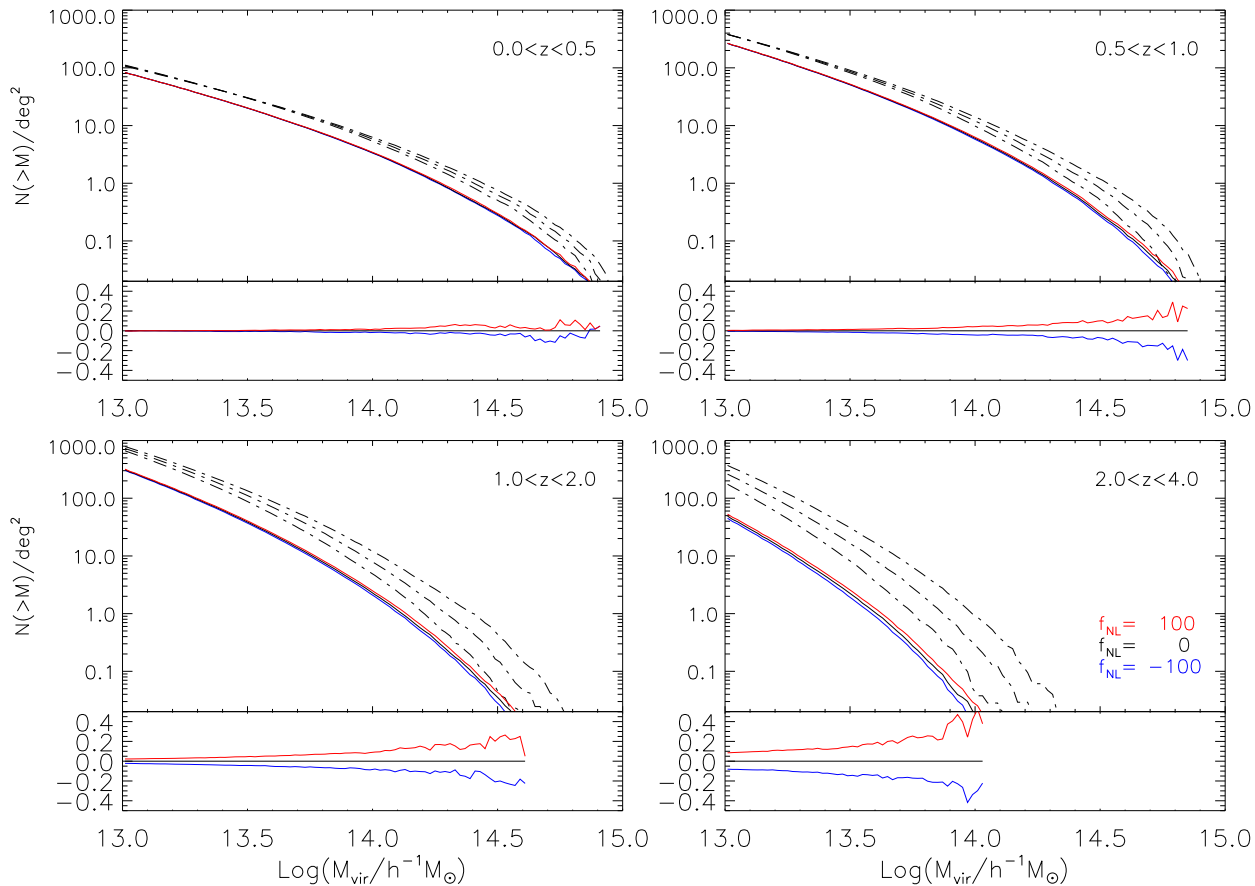


Figure 1. The log N -log M for the two simulation sets in different redshift bins. In the upper panels the solid lines refer to the first simulation set (average of 20 light-cone realizations) for the three different levels of non-Gaussianity: $f_{\text{NL}}=0, \pm 100$. The dot-dashed lines refer to the second simulation set (average of 100 light cones, *WMAP-I* cosmology) for models with $f_{\text{NL}}=0, \pm 1000$. In the lower panels we show, for the first set of simulations only, the difference $\Delta N/N$, computed with respect to the Gaussian ($f_{\text{NL}}=0$) simulation.

$10^{14}h^{-1}M_{\odot}$) cluster counts, which increases to about 10 per cent at $z > 1$. This is in agreement with the fact the modification of the distribution of the primordial density fluctuations primarily affects the formation of the biggest haloes at early epochs, as already discussed in Grossi et al. (2009).

When comparing the two simulation sets, it is clear that the differences between the various non-Gaussian scenarios are very small compared to the ones resulting from the change of the cosmological model. For example, even at $z > 1$ the $f_{\text{NL}}=100$ model of the first set adds only about 10 per cent counts to the Gaussian case ($M_{\text{vir}} > 10^{14}h^{-1}M_{\odot}$), while the *WMAP-I* cosmology scenario predicts more than three times as much objects. This fact highlights that the uncertainties with cosmological parameters, particularly with σ_8 , are critical when addressing the problem of detecting primordial non-Gaussianities in the LSS. More in the detail, analytical models of the mass functions (e.g. Sheth & Tormen 2002) predict that a difference of ± 0.01 in σ_8 produces a change of about 10 per cent in the total integrated counts ($M_{\text{vir}} > 10^{14}h^{-1}M_{\odot}$), raising to about 15 per cent at $z > 1$, where the f_{NL} parameter is expected to produce the most significant effects. This aspect will be considered in the following analyses.

It is worth to note also that for masses higher than $\approx 10^{14.5}h^{-1}M_{\odot}$ the mass functions of the second simulation set steepen and approach the first-simulation ones: this is an artificial effect produced by the smaller box size of the second simulation (500 instead of $1200h^{-1}$ Mpc). In fact this causes a loss of power

for perturbations at large scales, corresponding to a lower abundance of objects with high masses, and gives an indication of the range of validity of our simulation sets.

3 MODELING X-RAY COUNTS

Since our simulations consider only DM particles, in order to compare our results with present and future cluster surveys we need to define a model to associate the baryonic component to each DM halo. In particular we will focus here on modeling the X-ray emission (and the SZ signal, described in Section 4), exploiting observed and predicted scaling relations. As said in Section 2.1, our method provides the virial mass M_{vir} of our clusters, while often scaling relations are published using other mass definitions (like M_{200} , M_{500} and so on): therefore, in order to convert M_{vir} to the required value, we assume that our DM haloes follow a NFW density profile (Navarro et al. 1997) with a concentration parameter c given by the $c(M, z)$ relation proposed by Dolag et al. (2004). Notice that here we explicitly neglect the presence of any diffuse emission from the IGM associated to the warm-hot intergalactic medium (WHIM) and concentrate only on signals coming from galaxy clusters and groups. Even if the WHIM component is expected to contribute significantly to the total LSS signal, its presence is not expected to significantly affect the clusters count rate (see, e.g., Roncarelli et al. 006a).

In order to associate an X-ray luminosity to a DM halo we assume the phenomenological mass-luminosity relation found by Stanek et al. (2006), namely

$$\frac{L_X}{h_{70}^{-2} 10^{44} \text{ erg s}^{-1}} = L_{15,0} E(z)^s \left(\frac{M_{200}}{10^{15} h^{-1} M_\odot} \right)^p, \quad (2)$$

where L_X is the luminosity in the [0.1-2.4 keV] band and M_{200} is the mass of the cluster inside a radius enclosing 200 times the critical density $\rho_c(z)$ of the Universe at the redshift of the cluster. The normalization $L_{15,0}$ corresponds to the luminosity of an object with $M_{200} = 10^{15} h^{-1} M_\odot$ at $z = 0$. The term $E(z)$ represents the redshift evolution of the Hubble parameter,

$$E(z) = \Omega_m (1+z)^3 + \Omega_\Lambda \quad (3)$$

while the value of s is assumed to correspond to the self-similar evolution case, $s = 7/3$. The best-fit parameters $L_{15,0}$ and p depend on the assumed cosmological model. Stanek et al. (2006) publish their results assuming both $\Omega_m=0.24$ ($\ln L_{15,0} = 1.19$, $p = 1.46$) and $\Omega_m=0.30$ ($\ln L_{15,0} = 1.34$, $p = 1.59$), therefore we can take those values as a reference for our first and second simulation sets, respectively. We also take into account a scatter in the $L_X - M$ relation that we fix to 17 per cent, as measured by Reiprich & Böhringer (2002).

In this work we will determine the observed clusters fluxes in the [0.5-2 keV] and [0.5-5 keV] bands to compare our results with the abundances derived from *ROSAT* X-ray clusters survey (Rosati et al. 2002) and to predict the expected counts for the forthcoming *eROSITA* survey (Predehl et al. 2007), respectively. In order to calculate the band corrections, we need to assume the ICM temperature that determines the spectral distribution of the emitted radiation. For this purpose we consider our haloes as isothermal and we use the $M_{200} - T_{200}$ relation which Arnaud et al. (2005) obtained from a sample of ten nearby clusters observed with *XMM-Newton*, adding a self-similar redshift evolution. Notice that their sample covers the temperature range 2–9 keV, so we are forced to extend this relation to smaller objects, where a steepening of the $M_{200} - T_{200}$ relation is expected. In fact, Arnaud et al. (2005) obtain a slope higher of ~ 0.2 when restricting their sample only the hottest ($T > 3.5$ keV) clusters. Even if neglecting this effect may lead to an underestimate of the cluster temperatures for the small objects, we checked that it does not have a strong impact on our final results. For example, if we assume a further steepening of 0.2 in colder ($T < 2$ keV) clusters, this leads to a change of about 1 per cent in the faint-end of the $\log N - \log S$, and the relative differences between the non-Gaussian scenarios remain unchanged.

It is known that the ICM cools mainly via *bremsstrahlung* emission which is the main physical process responsible of the X-ray emission of galaxy clusters. Therefore we can model the emission of the gas assuming a free-free spectrum with a Gaunt factor $g(E/k_B) T_{200} = (E/k_B)^{-0.3}$ (see, e.g., Borgani et al. 1999, for more details). With this simplifying assumption we are neglecting the presence of other known emission processes like line-emission from metals, which can give a non-negligible contribution especially to low-temperature ($T \lesssim 2$ keV) clusters; however, for the reasons explained above, neglecting this process has no significant impact on our final results.

Once obtained the band correction f_{band} , we calculate the cluster flux in a given band as

$$S_{\text{band}} = \frac{L_X f_{\text{band}}}{4\pi d_L(z)^2}, \quad (4)$$

where $d_L(z)$ is the luminosity distance of the cluster.

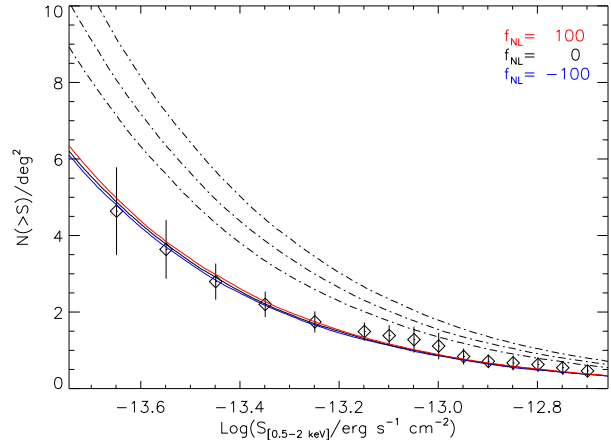


Figure 2. The number of haloes as a function of the flux limit in the [0.5-2 keV] band for the two simulation sets. The solid lines refer to the three models of the first set (average of 20 light-cone realizations) with $f_{\text{NL}}=0, \pm 100$. The dot-dashed line refer to the second simulation set (average of 100 light-cones, *WMAP-I* cosmology) for models with $f_{\text{NL}}=0, \pm 1000$. The diamonds with errorbars correspond to the number counts derived by Rosati et al. (2002) from *ROSAT* X-ray clusters survey.

Fig. 2 shows the number counts as a function of the X-ray flux limit in the [0.5-2 keV] band for the three models of the first set and for the $f_{\text{NL}}=0, \pm 1000$ of the second simulation set. Our results are compared with the counts obtained from the *ROSAT* survey, in the same band. All of the first three models show a good agreement with the data, having error bars much wider than the difference associated to the change of the f_{NL} parameter. On the contrary, the counts obtained with the *WMAP-I* cosmology are significantly higher (even when considering the standard Gaussian case): the only way to fit the data with these cosmological parameters would be to assume a strong negative evolution of the luminosity with redshift, e.g. adding an extra factor $(1+z)^\beta$ to equation 2, with $\beta \simeq -2$, which is absolutely unrealistic (see, e.g., Ettori et al. 2004). These results show that the dependence of the cluster counts on different cosmological parameters, and particularly on σ_8 , is much higher with respect to the one on the value of f_{NL} : this highlights the difficulty of constraining the level of the primordial non-Gaussianity with the current uncertainties in the cosmological parameters.

Fig. 3 shows the $\log N - \log S$ in the [0.5-5 keV] band in different redshift intervals. Again, the number counts differences between the different non-Gaussian scenarios are about one order of magnitude smaller than the corresponding differences obtained by increasing the value of σ_8 from 0.8 to 0.9. Anyway, it is interesting to note that in the redshift interval $0.5 < z < 1$, the number counts expected assuming the *eROSITA* detection limit (3.3×10^{-14} erg $\text{s}^{-1} \text{cm}^{-2}$) differ by about 10 per cent when assuming $f_{\text{NL}} = \pm 100$ with respect to the Gaussian model. These relative differences grow to about 20 per cent in the $1 < z < 2$ interval and increase for higher fluxes: this result is in agreement with the expected evolutionary scenario emerging from Fig. 1, with higher mass (and then more luminous) haloes forming earlier in models with positive f_{NL} .

Table 1 shows the number of galaxy clusters with $M_{200} > 10^{14} h^{-1} M_\odot$ that are expected to be detected by the *eROSITA* wide survey under our assumptions. For our predictions we assume an effective area of 20000 deg^2 and a detection limit of 3.3×10^{-14} erg $\text{s}^{-1} \text{cm}^{-2}$ in the [0.5-5 keV] band. For the Gaussian model we predict ~ 60000 detections, one per cent of them at redshift larger than

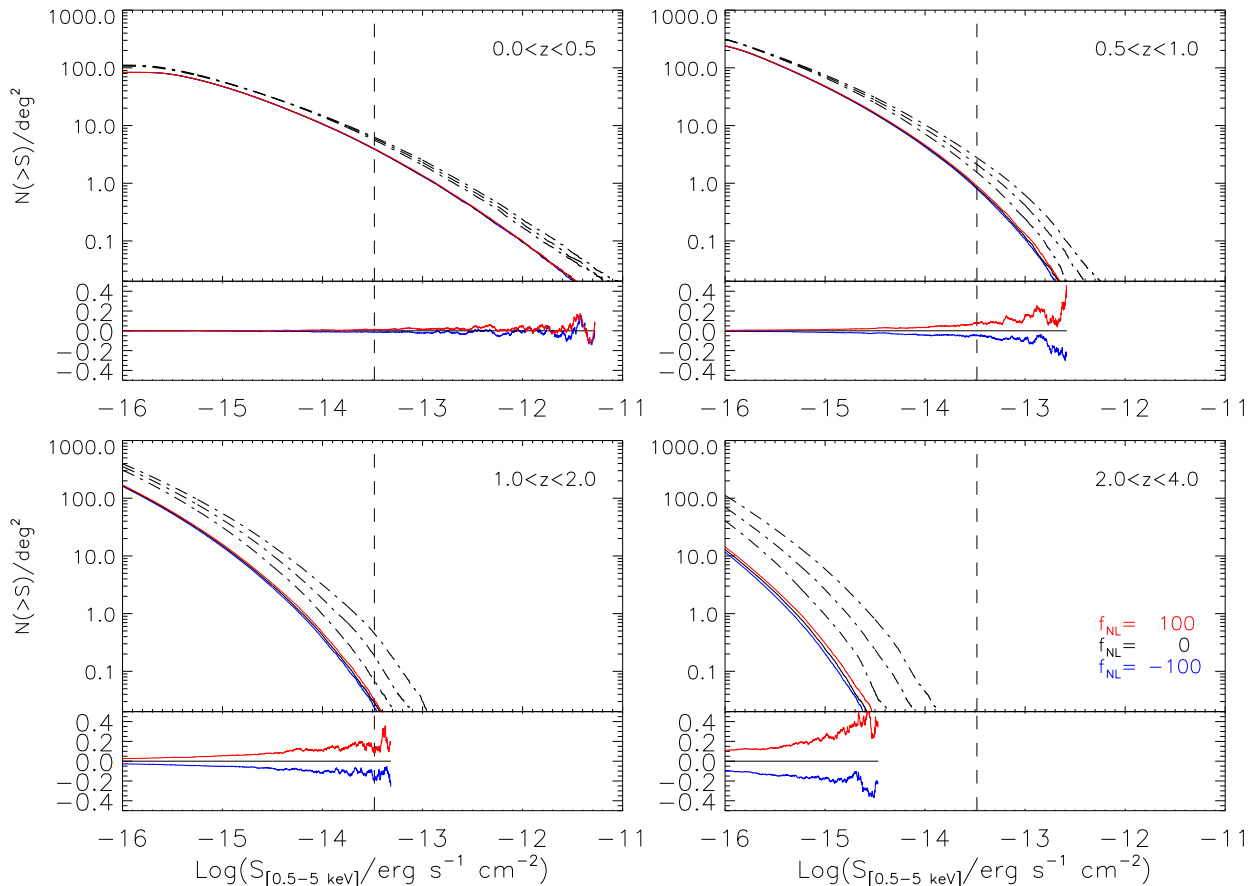


Figure 3. As in Fig. 1, but for the $\log N$ - $\log S$ in the [0.5-5 keV] band. The dashed vertical line indicates the *eROSITA* flux-limit, corresponding to 3.3×10^{14} $\text{erg s}^{-1} \text{cm}^{-2}$.

unity. The changes due to the presence of a moderate level of primordial non-Gaussianity ($f_{\text{NL}} = \pm 100$) are small, but always larger than the expected poissonian error: considering the total counts, the variation is about 4 per cent, while for the redshift bin $1 < z < 2$ the abundances change by 15 per cent. However, once again, the dependence on f_{NL} is much smaller when compared to the one on the power spectrum normalization σ_8 : at $z > 1$, the differences in the cluster counts associated to the $f_{\text{NL}} = \pm 100$ models are comparable to an uncertainty of ± 0.01 in σ_8 (see the discussion in Sect. 2.2). For what concerns the total integrated counts, the number of objects detectable by the *eROSITA* survey predicted by the Gaussian simulation of the second set ($\sigma_8 = 0.9$) grows by a factor of 2: ~ 120000 objects, with a similar redshift distribution. This confirms the necessity of having alternative derivations of the main cosmological parameters to allow to exploit the power of cluster counts to constrain the level of primordial non-Gaussianity (see also Fedeli et al. 2009).

4 THE THERMAL SZ EFFECT

Another important observable quantity to study galaxy clusters is the thermal SZ (tSZ) effect, namely the inverse-Compton scattering of the CMB photons caused by the electrons present in the hot intracluster plasma (see, e.g., Birkinshaw 1999; Carlstrom et al. 2002, for detailed reviews). This effect causes a distortion in the CMB blackbody spectrum, whose intensity in a given direction can be expressed in terms of the Compton y -parameter defined as

Table 1. The number of detected haloes (with $M_{200} > 10^{14} h^{-1} M_{\odot}$) predicted for the *eROSITA* wide survey in different redshift bins. The quoted errors are assumed to be poissonian.

f_{NL}	Number counts			Total
	$0 < z < 0.5$	$0.5 < z < 1$	$1 < z < 2$	
-100	41590 ± 204	15934 ± 126	478 ± 22	58007 ± 241
0	42318 ± 206	16715 ± 129	571 ± 24	59610 ± 244
100	43443 ± 208	18015 ± 134	641 ± 25	62105 ± 249

$$y \equiv \frac{k_{\text{B}} \sigma_{\text{T}}}{m_e c^2} \int n_e T_e dl ; \quad (5)$$

here k_{B} is the Boltzmann constant, σ_{T} is the Thomson cross section, m_e is the electron mass, c is the light speed, while n_e and T_e represent the electron number density and temperature, respectively. The distortion of the signal results in a difference ΔT in the measured temperature which depends on the observational frequency. In the Rayleigh-Jeans (RJ) limit this is given by

$$\frac{\Delta T}{T_{\text{CMB}}} = -2y, \quad (6)$$

where $T_{\text{CMB}} = 2.726$ K is the CMB temperature (Mather et al. 1994), thus producing a temperature decrement, which can be as high as $\Delta T \approx 10^{-3}$ K for the central regions of the most massive clusters.

Table 2. The number of detected haloes (with $M_{200} > 10^{14}h^{-1}M_{\odot}$) predicted for the *SPT* wide survey in different redshift bins. The quoted errors are assumed to be poissonian.

f_{NL}	Number counts			Total
	$0 < z < 0.5$	$0.5 < z < 1$	$1 < z < 2$	
-100	7796 ± 88	5961 ± 75	960 ± 31	14456 ± 120
0	7958 ± 89	6041 ± 78	1124 ± 34	15137 ± 123
100	8144 ± 90	6357 ± 80	1268 ± 36	15784 ± 126

Following an observationally oriented approach, the interesting quantity to be evaluated for a given halo is the integrated Compton y -parameter Y , defined as

$$Y \equiv \int_{\Omega} y d\Omega = \frac{1}{d_A^2(z)} \left(\frac{k_B \sigma_T}{m_e c^2} \right) \int_V n_e T_e dV, \quad (7)$$

where Ω is the solid angle subtended by the cluster and V is its physical volume. This adimensional quantity depends on the angular diameter distance $d_A(z)$, and constitutes an equivalent to the flux in the X-rays. Therefore it is useful to introduce the intrinsic Compton y -parameter defined as

$$Y^{\text{int}} \equiv Y d_A(z)^2, \quad (8)$$

which is roughly proportional to the mass and to the temperature of the object. Using hydrodynamical simulations it has been possible to calibrate scaling relations between the cluster mass and its SZ observables (see, e.g., Diaferio et al. 2005; Shaw et al. 2008): here we adopt the $M - Y^{\text{int}}$ relation, found by Nagai (2006), that can be expressed in the form

$$\frac{Y_{200}^{\text{int}}}{\text{Mpc}^2} = A_{14} \times 10^{-6} E(z)^s \left(\frac{M_{200}}{10^{14}h^{-1}M_{\odot}} \right)^{\alpha}, \quad (9)$$

where the pedex indicates that we are considering quantities computed inside the volume enclosed by R_{200} . By fitting the data computed from their simulated clusters sample, Nagai (2006) obtained $A_{14} = 2.56$ and $\alpha = 1.70$ (we consider the results of their CSF simulation, which accounts for a variety of physical processes of the baryonic component): we used this relation assuming, as we did for the X-ray modeling, a self-similar redshift evolution, corresponding for the tSZ effect to $s = 2/3$.

We show the results of our $\log N - \log Y^{\text{int}}$ in Fig. 4. Most of the conclusions derived from the analysis of the X-ray results apply also for the tSZ effect: the uncertainties in the estimate of σ_8 make it very challenging to discriminate between different non-Gaussian models. However it is worth to notice that, since the tSZ effect is not affected by redshift dimming as the X-ray flux, at higher redshifts ($z > 1$) the number of detections is still significant. For example, assuming the flux limit expected for the *SPT* survey (i.e. 5 mJy at 150 GHz, corresponding to $Y \simeq 3.4 \times 10^{-12}$, see Majumdar & Mohr 2003), we predict the possibility of detecting ~ 0.3 high- z objects per square degree: given the expected area of 4000 deg^2 , this leads to more than one thousand objects, enough to potentially discriminate the ~ 20 per cent difference in the cluster counts predicted for the $f_{\text{NL}} = \pm 100$ models. Note that these deviations are comparable to an uncertainty of about ± 0.02 in the primordial power spectrum normalization σ_8 . The expected number counts from the *SPT* survey in different redshift ranges are reported in Table 2.

4.1 Integrated properties of the tSZ signal

Apart from cluster counts, other global quantities like the average Compton y -parameter and the tSZ power spectrum can be affected by the presence of a non-Gaussian signature in the primordial power spectrum of perturbations. In order to study these observables, it is necessary to create and analyse mock maps of the y -parameter. Since galaxy clusters are extended sources, we need to make further assumptions about the density and temperature profiles of the haloes to model the distribution of the signal on the sky. Since the tSZ signal receives a significant contribution also from the external regions of galaxy clusters, the modelisation must take into account the steepening of the slope of these profiles in the regions around the virial radius (see, e.g., Vikhlinin et al. 2006; Roncarelli et al. 006b). In this context, it is important to note that a classic β -model (Cavaliere & Fusco-Femiano 1978) would fail simply because it does not converge for large distances from the centre, even when assuming a decrease of the temperature with a polytropic index, as adopted in Ameglio et al. (2006). Therefore, we start from the suggestion of Ameglio et al. (2006) and slightly modify their results by introducing a rolling- β polytropic profile for the tSZ signal, namely

$$y(\theta) = y_0 \left[1 + \left(\frac{\theta}{\theta_c} \right)^2 \right]^{-3\beta_{\text{eff}}(\gamma-1)/2}, \quad (10)$$

where θ is the angular separation from the cluster centre, θ_c is the angular size of the core radius (assumed to be $r_c = 0.1R_{200}$), $\gamma = 1.18$ is the polytropic index of the gas. The effective slope β_{eff} is given by

$$\beta_{\text{eff}} = -\beta_{\text{ext}} \left(\frac{x + \beta_{\text{int}}/\beta_{\text{ext}}}{x + 1} \right), \quad (11)$$

where $x \equiv \theta/\theta_c$ and β_{ext} and β_{int} are the external and internal slopes for the density profile, respectively. In this way we can tune these two parameters in such a way that this expression converges to the profile of Ameglio et al. (2006) (and to a β -model) in the inner part, while in the outer part it steepens to allow the value of the integrated Y^{int} to converge to a finite value ($\gamma\beta_{\text{ext}} > 1$). We choose $\beta_{\text{int}} = 2/3$ and $\beta_{\text{ext}} = 1.3$, where the latter value is taken in agreement with the analyses of Roncarelli et al. (006b) on the density profiles in the outskirts of simulated galaxy clusters. With this choice of parameters, the external part of our $y(\theta)$ profile also agrees with the results of Haugboelle et al. (2007). A visual comparison of these different profiles for Compton y -parameter is shown in the left panel of Fig. 5: while the three profiles converge to the same value at the centre, the rolling- β polytropic profile is significantly lower already at $\sim 3\theta_c$ ($\sim 0.3R_{200}$). When considering the distribution of the signal (right panel), it is easy to deduce that only with the profile adopted in this work Y^{int} converges to a finite value for high values of θ . It is worth to notice that even adopting this profile, the total signal up to R_{200} is only the 93 per cent of the total signal: this indicates that using any other shallower profile would lead to non-negligible biases.

Then we used this profile as a weight to distribute the total tSZ signal of each halo into the pixels of our maps. Since the adopted profile has non-zero contribution even at large scales, we set up the integration limit to the 99 per cent of the total value: this means integrating up to $\sim 2.3r_{200}$. We follow the procedure described in Roncarelli et al. (006a) to smooth the signal of the SPH particles and obtain the tSZ map corresponding to each simulated light-cone realization. At the end our analysis will be based on a total of 60 maps from the first simulation set and 700 from the second one. As

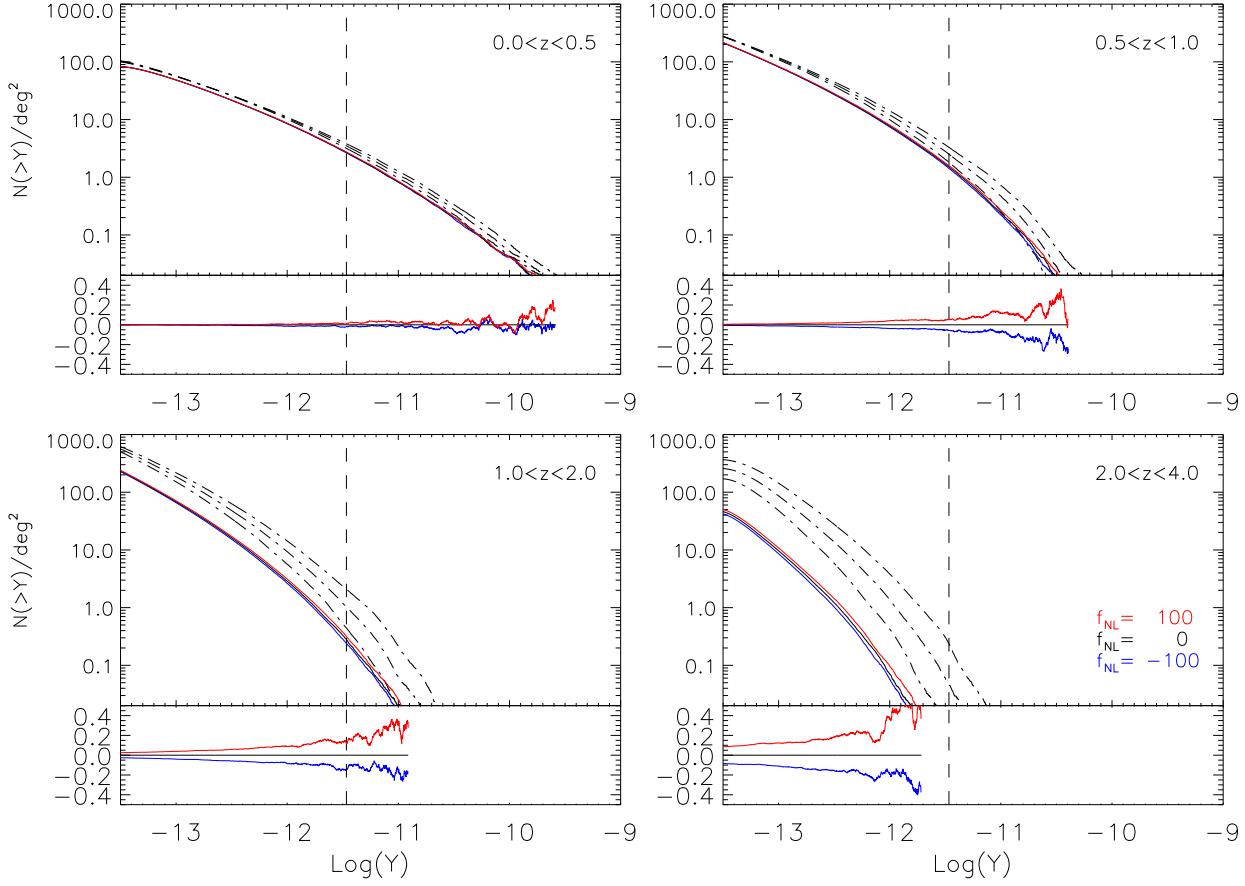


Figure 4. As in Fig. 1, but for the $\log N$ - $\log Y$. The dashed vertical line indicates the SPT flux-limit, i.e. 5 mJy at 150 GHz, corresponding to $Y \sim 3.4 \times 10^{-12}$.

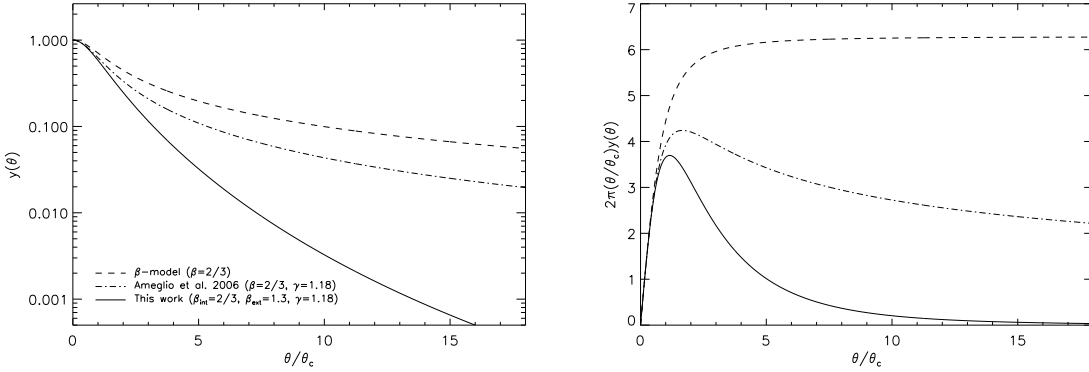


Figure 5. Left panel: comparison between the Compton y -parameter profiles for an isothermal β -model (dashed line), the polytropic β -model proposed by Arneglio et al. (2006) (dot-dashed line) and the rolling- β polytropic profile (solid line) used in this work. Right panel: distribution of the signal as a function of the distance from the centre for the same three profiles.

an example, in Fig. 6 we show the Compton y -parameter maps corresponding to the same light-cone realization, as obtained from the $f_{\text{NL}} = 0, \pm 1000$ simulations of the second set. With these extremely large amounts of primordial non-Gaussianity, it is possible to recognize the expected behavior: an evidence of more (less) clustered signal for positive (negative) f_{NL} , compared to the Gaussian case. Notice that the average value of the y -parameter computed over all the maps of the Gaussian simulation with the *WMAP-1* cosmology is $\langle y \rangle = 9.71 \times 10^{-7}$, while considering a *WMAP-3* cosmology (first set of simulations) this value drops to $\langle y \rangle = 5.22 \times$

10^{-7} , in good agreement with the expected scaling, $y \propto \Omega_{\text{m}} \sigma_8^{3.5}$ (see, e.g., Komatsu & Seljak 2002; Diego & Majumdar 2004). The last figure is also consistent with the results of Roncarelli et al. (2007) who, analysing a high-resolution hydrodynamical simulation (Borgani et al. 2004) based on the same cosmological model, obtained a value of $\langle y \rangle = 1.19 \times 10^{-6}$ with about half of the signal originated from the WHIM (not considered in this work). Notice that the mean values derived for the models with the *WMAP-3* cosmology but with $f_{\text{NL}} = 100$ and $f_{\text{NL}} = -100$ are $\langle y \rangle =$

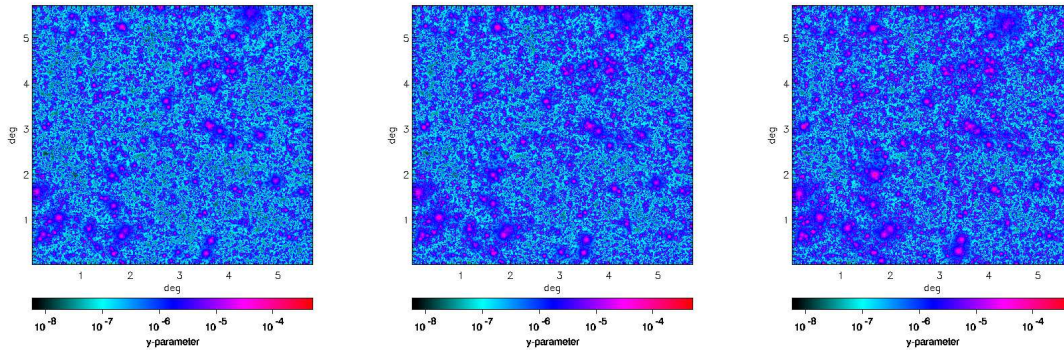


Figure 6. Examples of maps for the tSZ signal (expressed in terms of the Compton y -parameter) for three different levels of primordial non-Gaussianity, $f_{\text{NL}} = -1000, 0, 1000$ (left, center and right panels, respectively). These maps have been obtained from the second simulation set (*WMAP-1* cosmology): they are 5.71° on a side with a pixel size of $(20 \text{ arcsec})^2$. Notice that the three maps refer to the same light-cone realization.

5.37×10^{-7} and $\langle y \rangle = 5.08 \times 10^{-7}$, respectively, thus comparable within few percent to the Gaussian case.

4.2 Angular power spectrum

To characterize the statistical properties of the tSZ effect, it is important to study its power spectrum at different multipoles, in particular focusing on the angular scales at which the tSZ signal is expected to dominate the primary CMB anisotropies ($\ell \gtrsim 2000$). For the complete set of maps generated as described in the previous Section, we computed the tSZ power spectra, using a method based on Fast Fourier Transforms, adopting the approximation of flat sky (given the reduced extension of the maps) and assuming the RJ frequency limit. Finally, the corresponding averages are shown in Fig. 7 for the different models.

Again, when considering the first set of simulations, the differences between models with various values of f_{NL} are very low when compared to the variations related to a change of the cosmological scenario: about 10 per cent in both senses for the $f_{\text{NL}} = \pm 100$ models, compared to a factor of about 3 when changing σ_8 and Ω_m . This is expected as, given the dependence $C_\ell \propto \sigma_8^7$, the difference in the σ_8 choice accounts alone for a factor 2.3, with the remaining difference associated to the Ω_m parameter. For these reasons, the perspective of constraining f_{NL} seems to be quite demanding without an independent derivation of the main cosmological parameters.

The presence of a possible non-Gaussianity in post-inflationary perturbations has been also claimed by Sadeh et al. (2007) as a possible explanation of the anomalous values of the tSZ power spectrum obtained by the *BIMA* experiment. In particular, Dawson et al. (2002) measured an high value of $\Delta T = 16.6^{+5.3}_{-5.9} \mu\text{K}$ at $\ell = 5237$ (see, however, the smaller estimate obtained by Sharp et al. 2009, with the *SZA* experiment). According to our results, explaining the *BIMA* results with primordial non-Gaussian fluctuations alone (and keeping $\sigma_8 = 0.8$) would lead to values of f_{NL} unrealistically high ($f_{\text{NL}} \gg 100$). On the contrary, if slightly higher values of σ_8 are considered, the tSZ power spectrum would agree within 1σ with the result obtained by Dawson et al. (2002). In this context, a positive value of f_{NL} within current upper limits, could also contribute to boost the tSZ signal in order to explain these measurements.

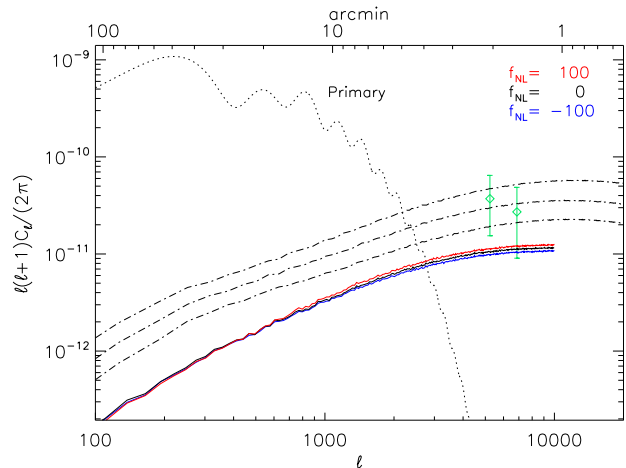


Figure 7. The power spectrum of the tSZ signal in the RJ limit as a function of the multipole ℓ for the two simulation sets. The solid lines refer to the first simulation set (average of the 20 light-cone realizations) for the three different levels of primordial non-Gaussianity ($f_{\text{NL}} = 0, \pm 100$), while the dot-dashed lines refer to the second simulation set (average of 100 light-cones, with *WMAP-1* cosmology) for $f_{\text{NL}} = 0, \pm 1000$. The dotted line represents the primary CMB signal calculated using CMBFAST (Seljak & Zaldarriaga 1996) adopting the *WMAP-3* cosmology. The diamonds with errorbars (1σ) represent the measurements of Dawson et al. (2002) with the *BIMA* experiment.

5 DIFFERENTIAL REDSHIFT COUNTS

From the results presented above it is clear that a significant detection of the signatures of a possible primordial non-Gaussianity based on global properties of galaxy clusters (e.g. number counts, mass functions, etc.) appears very difficult and well beyond the possibility of current and planned surveys. The main reason is not only the degeneracy of the results with other uncertain cosmological parameters (mostly σ_8), but also the fact that these observables are dominated by low-redshift haloes ($z \lesssim 0.5$) where the LSS properties of the different non-Gaussian models show smaller differences.

For these reasons the most reasonable strategy to break the degeneracy between f_{NL} and the other parameters can be a study of the evolution with redshift of the cluster counts. In Fig. 8 we show for the different models under analysis the redshift distribution of

the objects that will be detected by the *eROSITA* and *SPT* cluster surveys (left and right panels) in the X-ray and tSZ, respectively.

Looking in more detail at the *eROSITA* results, the cluster abundances at $z \gtrsim 0.5$, where the satellite is expected to detect about 15,000 objects (see Tab. 1), show a relative difference of about 10 per cent. Therefore, in principle, the possibility of estimating, thanks to a dedicated follow-up campaign, a high number of redshifts for the objects detected by *eROSITA* at $z > 0.5$, would allow to obtain their redshift distribution, increasing the chance of constraining f_{NL} , once the value of σ_8 is derived using the abundance of low-redshift objects.

A similar conclusion can be drawn by looking at the redshift distribution of the *SPT* clusters (right panel). The possibility of detecting very high-redshift ($z > 1$) clusters with an SZ survey is certainly promising, since in this redshift range the relative differences grows to ~ 20 per cent. However, the possibility of obtaining a significant amount of redshift estimates for these objects (which are ~ 1000 , see Section 4) is of course much lower, due to their lower signal.

6 CONCLUSIONS

In this work we used a set of cosmological N -body simulations to investigate the impact of primordial non-Gaussianity (parametrised in terms of f_{NL}) on the LSS. From their outputs we constructed halo catalogues at different redshifts and, making use of suitable scaling relations between masses and observables, we computed their expected X-ray emission and SZ signal. In particular we investigated the possibility of constraining f_{NL} with future projects, namely *eROSITA* and *SPT* cluster surveys. Moreover we discussed the degeneracy with other uncertain cosmological parameters, like Ω_{m} and σ_8 . Our main results can be summarised as follows.

(i) As predicted by analytical models (see, e.g., Matarrese et al. 2000; LoVerde et al. 2008), the main effects in cluster counts due to the presence of some level of primordial non-Gaussianity are for high masses and redshifts. In particular, for haloes with $M_{200} > 10^{14} h^{-1} M_{\odot}$ at $z > 1$, the differences with respect to the corresponding Gaussian models are about 20 per cent.

(ii) When the power spectrum normalization suggested by *WMAP-3* is adopted, models with a moderate level of non-Gaussianity ($f_{\text{NL}} = \pm 100$) well reproduce the observed cluster counts derived from *ROSAT* cluster survey. However, the dependence on f_{NL} is very weak, when compared to the one on σ_8 , which must be independently estimated to fully exploit cluster counts as a probe of primordial non-Gaussianity.

(iii) We predict the expected number and redshift distribution of the galaxy clusters that will be detected in two future cluster surveys: *eROSITA* (X-ray) and *SPT* (SZ). The effects due to a moderate primordial non-Gaussianity are in general of few per cent, reaching about 20 per cent only at high z . In general, the fact that it is easier to detect high- z objects with SZ observations, because of the absence of cosmological dimming, makes *SPT* a more promising probe for obtaining constraints on f_{NL} . However, once again, the results show a strong degeneracy between f_{NL} and other cosmological parameters. Similar conclusions can be also drawn when analysing the power spectrum of the tSZ signal produced by galaxy clusters.

(iv) On the whole, the best strategy to detect the signatures of primordial non-Gaussianity in the LSS is to perform deep cluster surveys, together with suitable optical follow-ups for the determination of their redshifts. With this kind of observational dataset, it

would be possible to constrain σ_8 using low-redshift objects and analyse the dN/dz in the range $0.5 \lesssim z \lesssim 1$ to constrain the value of f_{NL} . If with this method future surveys will allow to reduce the uncertainties on σ_8 to about 0.01, this would make possible to detect moderate non-Gaussianities of the order of $f_{\text{NL}} = \pm 100$ (see also Sefusatti et al. 2006; Oguri 2009).

In conclusion, the results of this paper confirm the power of statistical tests based on galaxy clusters as a probe for primordial non-Gaussianity. In particular the detection of objects in the high-mass tail at sufficiently large redshift, as possible in future SZ wide surveys like *SPT*, will be certainly useful to improve the constraints on f_{NL} coming from alternative methods, like CMB, ISW and galaxy biasing.

ACKNOWLEDGMENTS

Computations have been performed on the IBM-SP5 at CINECA (Consorzio Interuniversitario del Nord-Est per il Calcolo Automatico), Bologna, with CPU time assigned under an INAF-CINECA grant, and on the IBM-SP4 machine at the ‘‘Rechenzentrum der Max-Planck-Gesellschaft’’ at the Max-Planck Institut fuer Plasmaphysik with CPU time assigned to the ‘‘Max-Planck-Institut für Astrophysik’’ and at the ‘‘Leibniz-Rechenzentrum’’ with CPU time assigned to the Project ‘‘h0073’’. We acknowledge the support of grant ANR-06-JCJC-0141 and the DFG cluster of excellence Origin and Structure of the Universe. We also acknowledge partial support by ASI contract I/016/07/0 ‘‘COFIS’’, ASI-INAF I/023/05/0 and ASI-INAF I/088/06/0. We acknowledge useful discussions with S.Ameglio, S.Ettori and L.Verde.

REFERENCES

- Afshordi N., Tolley A. J., 2008, *Phys. Rev. D*, 78, 123507
- Ameglio S., Borgani S., Diaferio A., Dolag K., 2006, *MNRAS*, 369, 1459
- Arnaud M., Pointecouteau E., Pratt G. W., 2005, *A&A*, 441, 893
- Bartolo N., Komatsu E., Matarrese S., Riotto A., 2004, *Phys. Rep.*, 402, 103
- Baumann D., 2009, *ArXiv0907.5424*
- Baumann D., Peiris H. V., 2008, *ArXiv0810.3022*
- Birkinshaw M., 1999, *Phys. Rep.*, 310, 97
- Borgani S., et al., 2004, *MNRAS*, 348, 1078
- Borgani S., Rosati P., Tozzi P., Norman C., 1999, *ApJ*, 517, 40
- Carbone C., Verde L., Matarrese S., 2008, *ApJ*, 684, L1
- Carlstrom J. E., et al., 2009, *ArXiv0907.4445*
- Carlstrom J. E., Holder G. P., Reese E. D., 2002, *ARA&A*, 40, 643
- Cavaliere A., Fusco-Femiano R., 1978, *A&A*, 70, 677
- Dalal N., Doré O., Huterer D., Shirokov A., 2008, *Phys. Rev. D*, 77, 123514
- Dawson K. S., Holzapfel W. L., Carlstrom J. E., Joy M., LaRoque S. J., Miller A. D., Nagai D., 2002, *ApJ*, 581, 86
- Desjacques V., Seljak U., Iliev I. T., 2009, *MNRAS*, 396, 85
- Diaferio A., Borgani S., Moscardini L., Murante G., Dolag K., Springel V., Tormen G., Tornatore L., Tozzi P., 2005, *MNRAS*, 356, 1477
- Diego J. M., Majumdar S., 2004, *MNRAS*, 352, 993
- Dolag K., Bartelmann M., Perrotta F., Baccigalupi C., Moscardini L., Meneghetti M., Tormen G., 2004, *A&A*, 416, 853
- Ettori S., Tozzi P., Borgani S., Rosati P., 2004, *A&A*, 417, 13

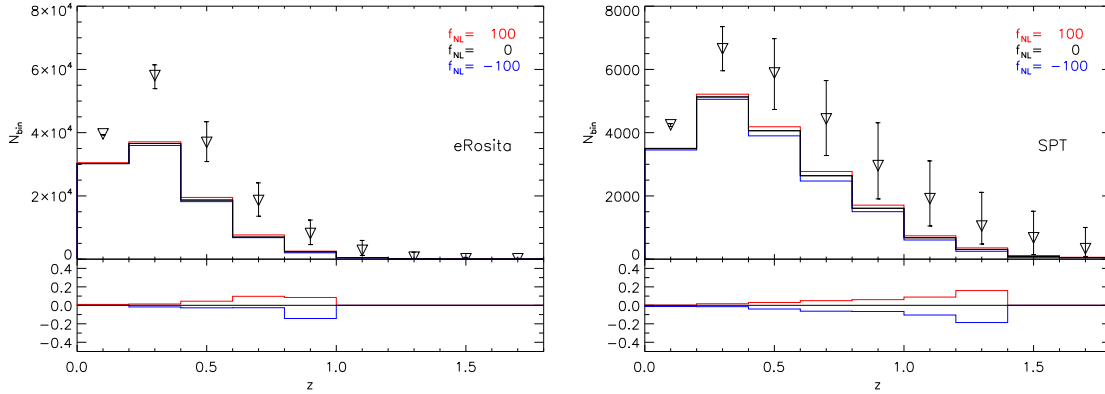


Figure 8. The predicted number counts (in different redshift bins with $\Delta z = 0.2$) of objects detected by *eROSITA* (flux limit of 3.3×10^{-14} erg s $^{-1}$ cm $^{-2}$ in the [0.5-5 keV] band; left panel) and *SPT* (flux limit corresponding to $S > 5$ mJy at 150 GHz; right panel). The solid lines refer to the first simulation set for the three different levels of non-Gaussianity: $f_{\text{NL}}=0, \pm 100$. The triangles correspond to the results of the Gaussian simulation of the second set, with errorbars indicating how the values change for the corresponding non-Gaussian models with $f_{\text{NL}} = \pm 1000$. In the lower panel we show, for the first set only, the difference $\Delta N/N$, computed with respect to the Gaussian ($f_{\text{NL}}=0$) simulation.

Fedeli C., Moscardini L., Matarrese S., 2009, MNRAS, 397, 1125
 Gangui A., Lucchin F., Matarrese S., Mollerach S., 1994, ApJ, 430, 447

Grossi M., Dolag K., Branchini E., Matarrese S., Moscardini L., 2007, MNRAS, 382, 1261

Grossi M., Verde L., Carbone C., Dolag K., Branchini E., Iannuzzi F., Matarrese S., Moscardini L., 2009, MNRAS, 398, 321

Haugboelle T., Sommer-Larsen J., Pedersen K., 2007, ArXiv0712.2453

Kang X., Norberg P., Silk J., 2007, MNRAS, 376, 343

Kinney W. H., 2008, International Journal of Modern Physics E, 17, 904

Komatsu E., Dunkley J., Nolte M. R., Bennett C. L., Gold B., Hinshaw G., Jarosik N., Larson D., Limon M., Page L., Spergel D. N., Halpern M., Hill R. S., Kogut A., Meyer S. S., Tucker G. S., Weiland J. L., Wollack E., Wright E. L., 2009, ApJS, 180, 330

Komatsu E., Seljak U., 2002, MNRAS, 336, 1256

Komatsu E., Spergel D. N., 2001, Phys. Rev. D, 63, 063002

Lam T. Y., Sheth R. K., 2009, MNRAS, pp 1112–+

Langlois D., 2008, ArXiv0811.4329

LoVerde M., Miller A., Shandera S., Verde L., 2008, Journal of Cosmology and Astro-Particle Physics, 4, 14

Maggiore M., Riotto A., 2009, ArXiv0903.1251

Majumdar S., Mohr J. J., 2003, ApJ, 585, 603

Matarrese S., Verde L., Jimenez R., 2000, ApJ, 541, 10

Mather J. C., et al., 1994, ApJ, 420, 439

McDonald P., 2008, Phys. Rev. D, 78, 123519

Messina A., Moscardini L., Lucchin F., Matarrese S., 1990, MNRAS, 245, 244

Moscardini L., Matarrese S., Lucchin F., Messina A., 1991, MNRAS, 248, 424

Nagai D., 2006, ApJ, 650, 538

Navarro J. F., Frenk C. S., White S. D. M., 1997, ApJ, 490, 493

Oguri M., 2009, Physical Review Letters, 102, 211301

Pillepich A., Porciani C., Hahn O., 2008, ArXiv0811.4176

Predehl P., et al., 2007, in Society of Photo-Optical Instrumentation Engineers (SPIE) Conference Series Vol. 6686 of Society of Photo-Optical Instrumentation Engineers (SPIE) Conference Series, eROSITA

Reiprich T. H., Böhringer H., 2002, ApJ, 567, 716

Roncarelli M., Moscardini L., Borgani S., Dolag K., 2007, MNRAS, 378, 1259

Roncarelli M., Moscardini L., Tozzi P., Borgani S., Cheng L. M., Diaferio A., Dolag K., Murante G., 2006a, MNRAS, 368, 74

Roncarelli M., Ettori S., Dolag K., Moscardini L., Borgani S., Murante G., 2006b, MNRAS, 373, 1339

Rosati P., Borgani S., Norman C., 2002, ARA&A, 40, 539

Sadeh S., Rephaeli Y., Silk J., 2007, MNRAS, 380, 637

Salopek D. S., Bond J. R., 1990, Phys. Rev. D, 42, 3936

Sefusatti E., Crocce M., Pueblas S., Scoccimarro R., 2006, Phys. Rev. D, 74, 023522

Seljak U., Zaldarriaga M., 1996, ApJ, 469, 437

Sharp M. K., Marrone D. P., Carlstrom J. E., Culverhouse T., Greer C., Hawkins D., Hennessy R., Joy M., Lamb J. W., Leitch E. M., Loh M., Miller A., Mroczkowski T., Muchovej S., Pryke C., Woody D., 2009, ArXiv0901.4342

Shaw L. D., Holder G. P., Bode P., 2008, ApJ, 686, 206

Sheth R. K., Tormen G., 2002, MNRAS, 329, 61

Slosar A., Hirata C., Seljak U., Ho S., Padmanabhan N., 2008, Journal of Cosmology and Astro-Particle Physics, 8, 31

Smith K. M., Senatore L., Zaldarriaga M., 2009, ArXiv0901.2572

Spergel D. N., et al., 2003, ApJS, 148, 175

Spergel D. N., et al., 2007, ApJS, 170, 377

Springel V., 2005, MNRAS, 364, 1105

Springel V., Yoshida N., White S. D. M., 2001, New Astronomy, 6, 79

Stanek R., Evrard A. E., Böhringer H., Schuecker P., Nord B., 2006, ApJ, 648, 956

Sunyaev R. A., Zel'dovich Y. B., 1972, Comments on Astrophysics and Space Physics, 4, 173

Sunyaev R. A., Zel'dovich Y. B., 1980, ARA&A, 18, 537

Valageas P., 2009, ArXiv0906.1042

Verde L., Matarrese S., 2009, ArXiv e-prints

Verde L., Wang L., Heavens A. F., Kamionkowski M., 2000, MNRAS, 313, 141

Viel M., Branchini E., Dolag K., Grossi M., Matarrese S., Moscardini L., 2009, MNRAS, 393, 774

Vikhlinin A., Kravtsov A., Forman W., Jones C., Markevitch M., Murray S. S., Van Speybroeck L., 2006, ApJ, 640, 691

Weinberg D. H., Cole S., 1992, MNRAS, 259, 652

Yadav A. P. S., Wandelt B. D., 2008, Physical Review Letters,

